Separation of the acoustic and aerodynamic wall pressure fluctuations

Alice Dinsenmeyer, Quentin Leclere, Jérôme Antoni

SEPARATION OF THE ACOUSTIC AND AERODYNAMIC WALL PRESSURE FLUCTUATIONS

Alice Dinsenmeyer[1,2] **Quentin Leclère**[1] **Jérôme Antoni**[1]
[1] Univ Lyon, INSA Lyon, LVA, F-69621 Villeurbanne, France
[2] Univ Lyon, École Centrale de Lyon, LMFA, UMR 5509, F-69134 Écully, France
alice.dinsenmeyer@insa-lyon.fr

ABSTRACT

Wall pressure measurements may results from two contributions: one coming from the acoustic sources and another induced by the turbulent boundary layer (TBL) pressure. An accurate separation of these two contributions may be required for two purposes: first, the extraction of the acoustic part is necessary for the quantification and the localization of the acoustic sources and second, the extraction of the TBL part is needed for the characterization of the vibro-acoustic excitation of the wall. In this paper, a post-processing method is proposed to perform this separation through a decomposition of the measured cross-spectral matrix using the statistical properties of the two contributions, especially their different spatial correlation structures. The approach is assessed on parietal pressure measurements acquired in a wind-tunnel with controlled sources and flow.

1. INTRODUCTION

When dealing with multichannel wall pressure measurements, one challenge is to discriminate the contribution coming from the aeroacoustic sources and the pressure fluctuations induced by the turbulent boundary layer (TBL). An accurate separation of these two contributions offers a twofold perspective. On the one hand, a correct estimation of the acoustic part is required for an appropriate quantification and localization of the aeroacoustic sources. On the other hand, the characterization of the TBL part allows a better understanding of the vibro-acoustic excitation, with applications such as the prediction of the vehicle interior noise.

Many techniques are used to perform this separation. When it is possible, the contribution of the TBL part can be mitigated by the use of physical filtering such as wind screens [1], microphone recession [2] or structural vibration measurements [3], but a residual TBL part might still contaminate the acoustic measurements. Wavenumber filtering is also widespread [4], but it requires a dense array and a clear separation of the acoustical and TBL wavenumber contents, which is not the case at low frequencies.

In this paper, a post-processing approach is proposed, that relies on a decomposition of the measured cross-spectral matrix (CSM) into acoustic and aerodynamic CSMs by means of the prior knowledge about the inherent correlation structure of each contribution. This matrix decomposition is written as a constrained optimization problem, solved within a Bayesian framework. The two contributions are thus estimated jointly according to their statistical model. Section 2 is dedicated to the presentation of this method.

Then, in section 3, the proposed separation approach is assessed on parietal pressure measurements performed in a wind-tunnel with controlled acoustic sources and with an array specifically designed for acoustic source localization.

2. SEPARATION USING STOCHASTIC MODELING

The separation approach described in this section is an extension of the Probabilistic Factor Analysis model that has been previously applied to the denoising of aeroacoustic measurements [5, 6, 3, 7]. This extension integrates a correlated noise model for the identification of the TBL noise contribution, and it is further called PFA-Corr.

2.1 Problem statement

In order to state the problem, let us first introduce the vector of measurements $\boldsymbol{y}_j$ that concatenates the Fourier coefficients for each sensor at one frequency and one snapshot j. As said previously, these measurements results from the sum of a contribution coming from the acoustic sources written $\boldsymbol{a}_j$ and another major contribution induced by the TBL noise, written $\boldsymbol{n}_j$. Adding also a minor contribution that models the other sources of noise ϵ_j, the sum of all the contributions reads

$$\boldsymbol{y}_j = \boldsymbol{a}_j + \boldsymbol{n}_j + \epsilon_j \tag{1}$$

This measured field is supposed to be statistically stationary in time, and thus an estimate of the CSM is obtained by averaging over N_s snapshots at a given frequency:

$$\hat{\boldsymbol{S}}_{yy} = \frac{1}{N_s} \sum_{j=1}^{N_s} \boldsymbol{y}_j \boldsymbol{y}_j^H \tag{2}$$

where the superscript H is the conjugate transpose operator. Assuming that the three terms in the sum (1) are statistically uncorrelated, the theoretical CSM (obtained at the limit when the number of snapshots tends to infinity) can

be decomposed as follows:

$$\boldsymbol{S}_{yy} = \boldsymbol{S}_{aa} + \boldsymbol{S}_{nn} + \boldsymbol{S}_{\epsilon\epsilon}. \quad (3)$$

The separation method proposed in this paper performs jointly the identification of each CSM of this sum. In order to make this inverse problem identifiable, some constraints must be added to the model, by using the statistical properties of each CSM.

First, dealing with classical microphone arrays, the number of sources is supposed to be small compared to the number of sensors, and the acoustic field to have a high correlation length compared to the microphone interspacing. Therefore, the measured acoustical field can be described by a few unobserved latent variables, which reads

$$\boldsymbol{a}_j = \boldsymbol{L}\boldsymbol{c}_j, \quad (4)$$

with $\boldsymbol{c}_j$ the complex vector of $K \leq M$ latent variables and $\boldsymbol{L} \in \mathbb{C}^{M\times K}$ an unknown mixing matrix, and using the CSM notation:

$$\boldsymbol{S}_{aa} = \boldsymbol{L}\boldsymbol{S}_{cc}\boldsymbol{L}^H. \quad (5)$$

Then, another constrain that can be added to the model concerns the CSM of the TBL contribution. Several physical models in the frequency-space domain exist among which the Corcos' one [8] is chosen for our application because it has a low number of empirical parameters to set. Therefore, the statistical model for the covariance of the TBL noise for a pair of microphones (k, l) with coordinates (x_l, y_l) and (x_k, y_k), at a frequency f is

$$\boldsymbol{S}_{nn_{kl}} = p^2\, \mathrm{e}^{-\frac{2\pi f}{U_c}(\alpha_x|x_k-x_l|+\alpha_y|y_k-y_l|-\imath(x_k-x_l))}, \quad (6)$$

with $k, l = 1, \ldots, M$. In this model, the flow is supposed to be oriented along the x direction. The amplitude term p^2 is a real positive scalar. The parameters α_x and α_y stand for the longitudinal and transverse coherence decay rates and U_c is the vortex convection velocity. These three Corcos parameters α_x, α_y and U_c are determined from the measurements. To do so, the procedure proposed by Arguillat *et al.* [2] is followed: a Non-Linear Least Squares (NLLS) data-fitting is performed, providing a different parameter set at each frequency.

Finally, the third contribution to the measurements modeled in Eq. (1) is the additive random noise, that is supposed uncorrelated over the microphones. This can be statistically modeled by a diagonal CSM:

$$\boldsymbol{S}_{\epsilon\epsilon} = \lceil \boldsymbol{\sigma}_\epsilon^2 \rfloor \quad (7)$$

where the notation $\lceil \boldsymbol{u} \rfloor$ refers to a diagonal matrix with the vector $\boldsymbol{u}$ as diagonal elements.

2.2 Bayesian inference

Seeing all the unknown parameters of the fitting model as random variables, the problem can be solved by a Bayesian inference approach. Especially, the optimal parameters can be found through a maximization of the posterior Probability Density Function (PDF), which reads

$$\boldsymbol{\Theta}^\star = \mathrm{argmax}\left[\boldsymbol{\Theta} \mid \hat{\boldsymbol{S}}_{yy}\right] \quad (8)$$

with $\boldsymbol{\Theta}$ the set of the parameters to be inferred. The notation $[x \mid y]$ stands for the conditional PDF of x given y. In Bayesian approaches, all the parameters are assigned a prior PDF that accounts for all the prior knowledge about them. In Table 1 are given all the priors used for the application of the present paper. The choice of these priors is classical, with Gaussian priors on all the parameters except for variance parameters that are assigned an Inverse-Gamma prior (see Ref. [9], p.42-43 for more details). In this Table, the prior variance of the TBL CSM is

$$\boldsymbol{\Sigma}^2_{n_{kl}} = \mathrm{e}^{-\frac{2\pi f}{U_c}(\alpha_x|x_k-x_l|+\alpha_y|y_k-y_l|-\imath(x_k-x_l))}, \quad (9)$$

as described in Eq. (6).

Note that it is expected that the inferred TBL CSM $\boldsymbol{S}_{nn}$ does not exactly follow a classical Corcos' model, but has rather a correlation structure derived from a Corcos' model, corrected through 2 mechanisms. First, unlike the classical model, the Corcos' parameters are allowed to vary with frequency, which is known to be more consistent with real measurements [10]. Then, a second correction mechanism is induced by the fact that the Corcos model is only implied in the prior covariance of the TBL CSM. However, this CSM is inferred entirely from its posterior, which is itself proportional to the prior times the likelihood:

$$[\hat{\boldsymbol{S}}_{nn} \mid \infty] \propto [\hat{\boldsymbol{S}}_{nn}][\hat{\boldsymbol{S}}_{yy} \mid \infty] \quad (10)$$

where ∞ indicates all the other variables of the model. Therefore, the Corcos model is only a prior, and the inferred TBL CSM is also driven by the data through the likelihood $[\hat{\boldsymbol{S}}_{yy} \mid \infty]$. In other words, the inferred CSM is expected to be inspired by a Corcos' model, but corrected to best fit the data.

As the posterior PDF to maximize in Eq. (8) has no closed-form, it is estimated through a Monte Carlo Markov Chain algorithm [11, 7].

2.3 Assessment of the separation using wavenumber beamforming

In the following, an applications of the separation method is presented. In order to evaluate the performance of the separation, a wavenumber beamforming is performed on each identified CSM. The beamforming output corresponds to the projection of the measurements on the contribution of a given wave. Here, plane waves are used. Therefore, the output of the beamformer, at a point of coordinate (k_{x_i}, k_{y_i}) and at one frequency, can be written in a quadratic and vectorized form as follows:

$$A_i = \mathrm{vec}\big(\boldsymbol{w}_i\boldsymbol{w}_i^H\big)^H \mathrm{vec}(\boldsymbol{S}) \quad (11)$$

with $\boldsymbol{S}$ the CSM of interest and

$$\boldsymbol{w}_i = \mathrm{e}^{\imath k_{x_i}\boldsymbol{\delta x} + \imath k_{y_i}\boldsymbol{\delta y}}. \quad (12)$$

In the following, this beamforming is only applied on the cross-spectra of $\boldsymbol{S}$.

The wavenumber content of the acoustic contribution is expected to be located inside the acoustic circle, distorted

Priors	Hyper-priors	Inputs
$[\boldsymbol{L}] = \mathcal{N}_{\mathbb{C}}(\boldsymbol{0}, \boldsymbol{I}_{MK}/K)$		
$[\boldsymbol{c}] = \mathcal{N}_{\mathbb{C}}(\boldsymbol{0}, \lceil \boldsymbol{\sigma_c}^2 \rfloor)$	$[\boldsymbol{\sigma}_c^2] = \mathcal{IG}(\boldsymbol{a}_c, \boldsymbol{b}_c)$	$\boldsymbol{a}_c, \boldsymbol{b}_c = 10^{-3}$
$[p] = \mathcal{N}_{\mathbb{C}}(a_p, b_p)$		$a_p = (\mathrm{Trace}(\hat{\boldsymbol{S}}_{yy})/M)^{\frac{1}{2}}$ and $b_p = a_p/2$
$[\boldsymbol{n}] = \mathcal{N}_{\mathbb{C}}\left(\boldsymbol{0}, \boldsymbol{\Sigma}_n^2\right)$		U_c, α_x, α_y from NLLS
$[\boldsymbol{\sigma}_\epsilon^2] = \mathcal{IG}(\boldsymbol{a}_\epsilon, \boldsymbol{b}_\epsilon)$		$\boldsymbol{a}_\epsilon, \boldsymbol{b}_\epsilon = 10^{-3}$

Table 1: Prior PDFs assigned to each parameter and hyperparameter of the PFA-Corr model. $\mathcal{N}_{\mathbb{C}}$ stands for the multivariate complex normal distribution and $\mathcal{IG}$ is the inverse-gamma distribution. The input parameters U_c, α_x and α_y are given by a least mean squares procedure.

by the convection effects. The acoustic domain is bounded as follows [12]:

$$k_x = \frac{2\pi f \cos\theta}{c_0 + U_c \cos\theta} \quad \text{and} \quad k_y = \frac{2\pi f \sin\theta}{c_0 + U_c \cos\theta} \tag{13}$$

with $0 \leq \theta \leq 2\pi$ and c_0 the speed of sound in the ambient air at rest.

Concerning the TBL wavenumber content, it is expected to be centered on the convection wavenumber, at $k_x = \frac{2\pi f}{U_c}$. Depending on the frequency and the width of the TBL domain (given by the coherence-loss), the acoustic and TBL domains may overlap.

3. APPLICATION TO WIND-TUNNEL MEASUREMENTS

3.1 Experimental setup

The measurements are performed in a closed-section wind-tunnel at École Centrale de Lyon (LMFA laboratory), shown in Fig. (1a). As shown on the sketch in Fig. 1b, two sources are mounted in the ceiling of the test-section, excited by two uncorrelated white noises. An array composed of 73 MEMS microphones is mounted in the floor of the section, arranged as shown on Fig. 1c. The microphone inter-spacings vary from 0.2 cm to 27.4 cm. The acquisitions are performed synchronously, during 30 s, and the CSM are computed with a frequency resolution of 16 Hz, and 66 % overlapping rate.

Three measurements are performed with the MEMS array:

- **configuration A**: with the sources switched on and without flow,
- **configuration T30**: without sources and with a flow at 30 m/s,
- **configuration AT30**: with the sources switched on and the flow at 30 m/s.

The objective is to separate the acoustic and TBL contributions from the measurements AT30 and compare with the baseline measurements A and T30. Note that the proposed separation process does not compensate for the convection effect on the acoustic part. Therefore, the identified acoustic part cannot be similar to the non-convected measurement A.

Another measurement is also performed in the same wind-tunnel using a dense rotating linear array in place of the MEMS array. This array is made of 63 remote microphones spaced by 1 mm. The measurement is performed only in the T30 configuration and for three angular positions: parallel, normal and at $\pi/2$ rad from the flow axis. The records last 60 s, and the CSM are computed with a 4 Hz resolution, and 66% overlapping rate. As this type of array is much denser than the MEMS one, it is supposed to be more appropriate to characterize the TBL.

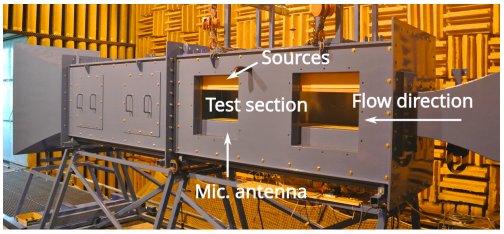

(a) Picture of the facility

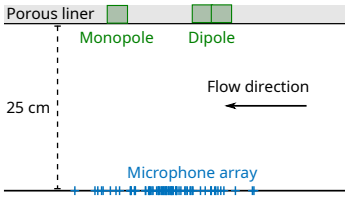

(b) Sketch of the test section (side view)

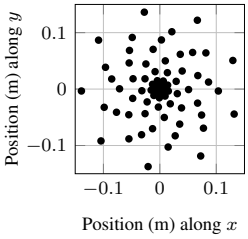

(c) Array design

Figure 1: Description of the experimental setup for the wind-tunnel measurements.

3.2 Beamforming maps of the measurements

The wavenumber content of the measurements is shown in the form of a k_x-k_y map at 2096 Hz in Fig 2. On these maps is plotted in black the convected acoustic circle. At this frequency, the acoustic and TBL domains are clearly visible, without overlapping. The wavenumber content is also shown in the form of a k_x-f map, at $k_y = 0$, in Fig. 3. On these maps is also plotted the acoustic circle, that appears as a cone nearly centered on $k_x = 0$. These maps show that the two domains overlap below 500 Hz. At low frequencies, the convective ridge is duplicated along the k_x axis because of aliasing effects. This aliasing is also visible around 2500 Hz, on the map of the configuration A, leading to some duplications of the acoustic spot. It is

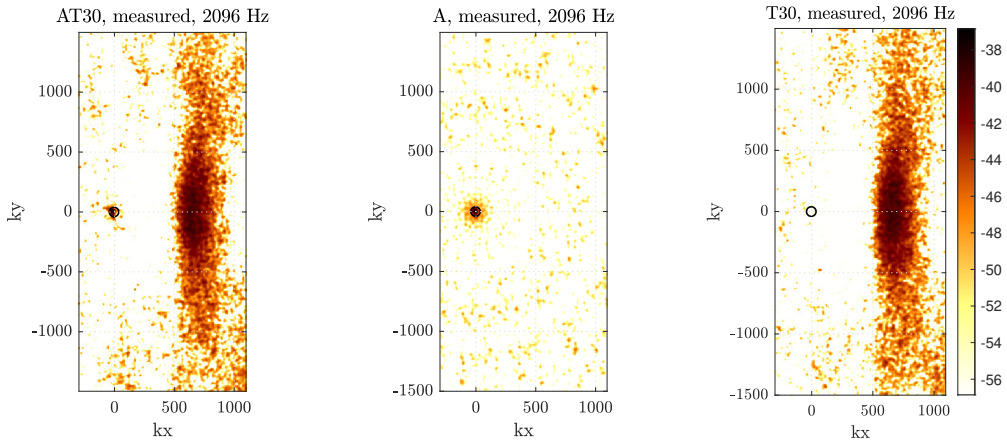

(a) AT30 configuration (b) A configuration (c) T30 configuration

Figure 2: Beamforming maps obtained at 2096 Hz **from the measurement** configurations AT30 (left), A (center), T30 (right), using the MEMS array. The 3 maps are scaled with the same color bar (in dB). The circle indicates the convected acoustic domain.

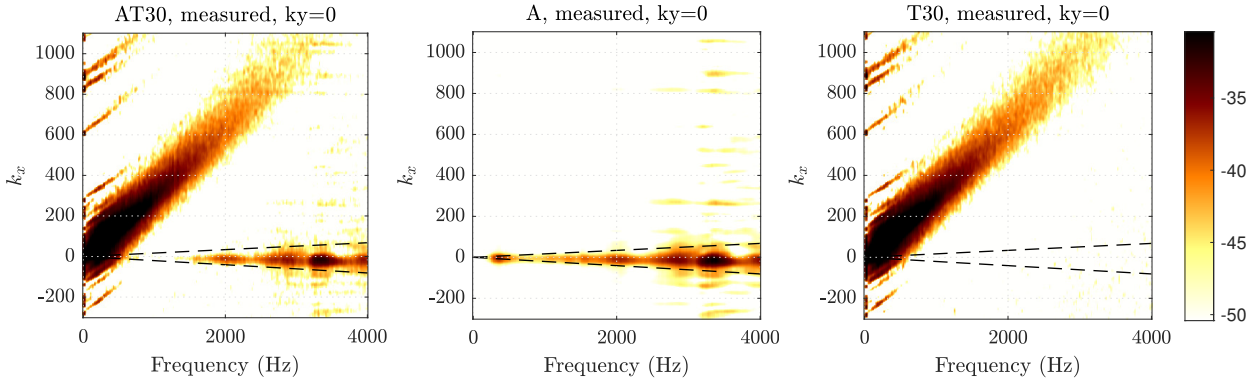

(a) AT30 configuration (b) A configuration (c) T30 configuration

Figure 3: Beamforming maps, as a function of the frequency at $k_y = 0$, **from the measurement** configurations AT30 (left), A (center), T30 (right), using the MEMS array. The 3 maps are scaled with the same color bar (in dB). The two dashed lines indicate the acoustic domain.

also clear that the order of magnitude of each component is very different depending on the frequency.

3.3 Estimation of the TBL parameters

In order to estimate the Corcos parameters required to apply the separation process, the NLLS regression is performed on the measurements. First, the measurement from the rotating array, at configuration T30, is used, because this array is supposed to be reliable for the characterization of the TBL. Then, NLLS is also applied on the MEMS measurements, at configuration AT30 to see if the strategy can be applied on measurements acquired with a less dense array and the in presence of an acoustic field.

In Fig. 4 are plotted the estimated parameters from the two datasets, as a function of the frequency. The longitudinal (along the stream direction, following the x-direction) and transverse (normal to the stream, along y-direction) correlation lengths are calculating as:

$$L_{c_{x,y}} = \frac{U_c}{2\pi f \alpha_{x,y}}. \tag{14}$$

The two arrays and configurations give very similar results at low frequency, but above 5 kHz, the inter-spacing of the MEMS microphones is to high to provide an accurate estimate. The estimated convection speed follows a classical decrease, as described in the literature [2, 10]. Similarly, the evolution of the correlations lengths with frequency is well known [13].

3.4 PFA-Corr separation results

Now that the Corcos parameters are estimated, the separation using PFA-Corr can be applied to the AT30 measurements. The beamforming maps of the inferred acoustic and TBL contribution are shown in Fig. 5.

On the inferred acoustic part, the convected ridge is totally absent, except below 220 Hz, where the TBL noise

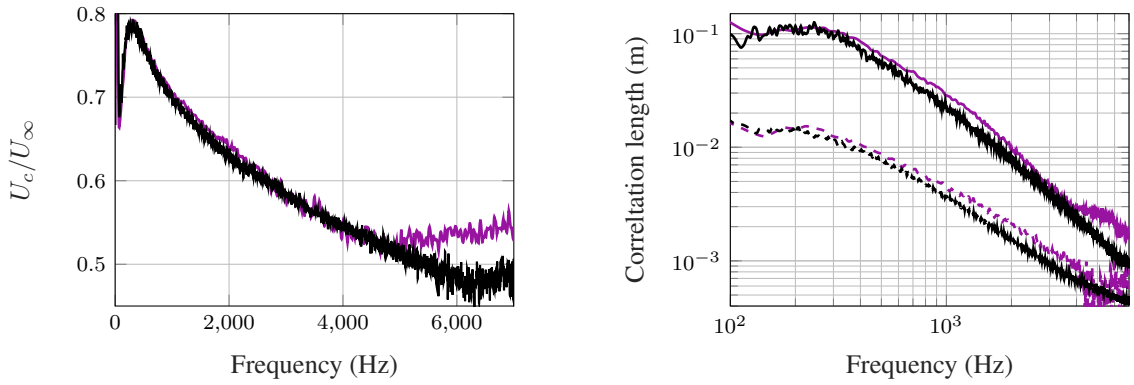

(a) Normalized convection speed

(b) Longitudinal (solid line) and transverse (dashed line) correlation lengths

Figure 4: Convection speed normalized by the flow speed U_∞ (a), longitudinal (solid line) and transverse (dashed line) correlations lengths (b) estimated using NLLS on the measurements with the rotating array (——) and with the MEMS array (——).

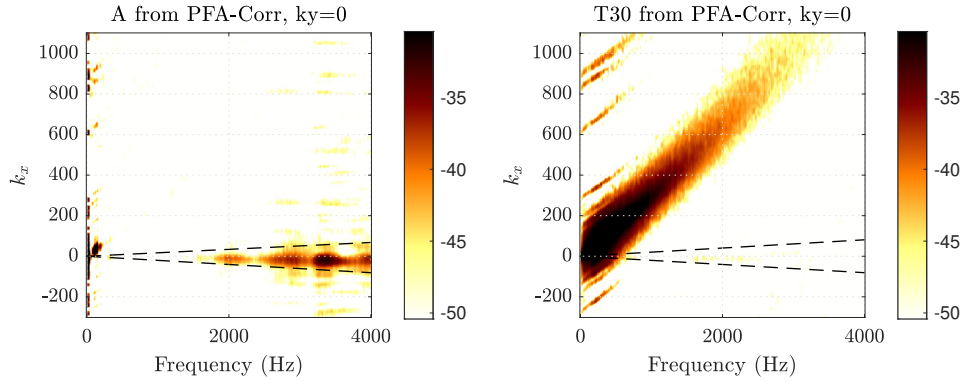

(a) Acoustic part

(b) TBL part

Figure 5: Beamforming maps obtained at $k_y = 0$ **from the PFA-Corr denoising** applied to the AT30 measurements. Identification of the acoustic part (left) and the TBL contribution (right). The 2 maps are scaled with the same color bar (in dB). The two dashed lines indicate the acoustic domain.

is highly correlated over the microphones and where the sources emit at very low amplitudes. Below 1500 Hz, the acoustic contribution seams to be not well reconstructed, but this should be confirmed by advanced acoustic imaging (in space). Similarly, the acoustic contribution appears to be fully separated from the TBL on Fig. 5b, which could also be verified by an imaging processing.

4. CONCLUSION

The separation of the TBL and acoustic contributions can be performed by a matrix decomposition, regularized by a Bayesian approach. In this inverse problem, a low rank model is assumed for the acoustic contribution, whereas a Corcos model is used to account for the prior TBL spatial correlation.

The Corcos model requires three empirical parameters that can be estimated experimentally, or by a simple least squares regression on the measurements, even with an array designed for the acoustic localization (*i.e.* not very dense) and in the presence of an acoustic field.

5. ACKNOWLEDGEMENTS

This work was performed within the framework of the Labex CeLyA of Université de Lyon, operated by the French National Research Agency (ANR-10-LABX-0060/ANR-16-IDEX-0005), and of the Clean Sky 2 Joint Undertaking, European Union (EU), Horizon 2020, CS2-RIA, ADAPT project, Grant agreement no 754881.

6. REFERENCES

[1] S. Jaeger, W. Horne, and C. Allen, "Effect of surface treatment on array microphone self-noise," in *6th AIAA/CEAS Aeroacoustics Conference*, p. 1937, 2000.

[2] B. Arguillat, D. Ricot, C. Bailly, and G. Robert, "Measured wavenumber: Frequency spectrum associated with acoustic and aerodynamic wall pressure fluctua-

tions," *The Journal of the Acoustical Society of America*, vol. 128, no. 4, pp. 1647–1655, 2010.

[3] Q. Leclere, A. Dinsenmeyer, E. Salze, and J. Antoni, "A comparison between different wall pressure measurement devices for the separation and analysis of tbl and acoustic contributions," in *Flinovia-Flow Induced Noise and Vibration Issues and Aspects*, Springer, 2019. (In press).

[4] E. Salze, E. Jondeau, A. Pereira, S. L. Prigent, and C. Bailly, "A new mems microphone array for the wavenumber analysis of wall-pressure fluctuations: application to the modal investigation of a ducted low-mach number stage," in *25th AIAA/CEAS Aeroacoustics Conference*, p. 2574, 2019.

[5] A. Dinsenmeyer, J. Antoni, Q. Leclere, and A. Pereira, "On the denoising of cross-spectral matrices for (aero) acoustic applications," in *Berlin Beamforming Conference*, no. BeBeC-2018-S2, 2018.

[6] A. Dinsenmeyer, Q. Leclere, J. Antoni, and E. Julliard, "Comparison of microphone array denoising techniques and application to flight test measurements," in *25th AIAA/CEAS Aeroacoustics Conference*, p. 2744, 2019.

[7] A. Dinsenmeyer, J. Antoni, Q. Leclere, and A. Pereira, "A probabilistic approach for cross-spectral matrix denoising: Benchmarking with some recent methods," *The Journal of the Acoustical Society of America*, vol. 147, no. 5, pp. 3108–3123, 2020.

[8] G. M. Corcos, "Resolution of pressure in turbulence," *The Journal of the Acoustical Society of America*, vol. 35, no. 2, 1963.

[9] A. Gelman, J. B. Carlin, H. S. Stern, D. B. Dunson, A. Vehtari, and D. B. Rubin, *Bayesian data analysis*. Chapman and Hall/CRC, 2014.

[10] H. H. Schloemer, "Effects of pressure gradients on turbulent boundary-layer wall-pressure fluctuations," *The Journal of the Acoustical Society of America*, vol. 40, no. 5, pp. 1254–1254, 1966.

[11] D. Gamerman and H. F. Lopes, *Markov chain Monte Carlo: stochastic simulation for Bayesian inference*. Chapman and Hall/CRC, 2006.

[12] L. Koop and K. Ehrenfried, "Microphone-array processing for wind-tunnel measurements with strong background noise," in *14th AIAA/CEAS Aeroacoustics Conference (29th AIAA Aeroacoustics Conference)*, p. 2907, 2008.

[13] T. M. Farabee and M. J. Casarella, "Spectral features of wall pressure fluctuations beneath turbulent boundary layers," *Physics of Fluids A: Fluid Dynamics*, vol. 3, no. 10, pp. 2410–2420, 1991.